ACS Catalysis

Research Article

pubs.acs.org/acscatalysis

In Situ-Generated Co^0-Co_3O_4/N-Doped Carbon Nanotubes Hybrids as Efficient and Chemoselective Catalysts for Hydrogenation of Nitroarenes

Zhongzhe Wei,[‡] Jing Wang,[‡] Shanjun Mao, Diefeng Su, Haiyan Jin, Yihe Wang, Fan Xu, Haoran Li, and Yong Wang*

Advanced Materials and Catalysis Group, ZJU-NHU United R&D Center, Department of Chemistry, Zhejiang University, Hangzhou 310028, P. R. China

Supporting Information

ABSTRACT: The earth-abundant nanohybrids Co^0/Co_3O_4@N-doped carbon nanotubes were fabricated via an efficient thermal condensation of D-glucosamine hydrochloride, melamine, and $Co(NO_3)_2 \cdot 6H_2O$. The hybrids furnish excellent catalytic activity and perfect chemoselectivity (>99%) for a wide range of substituted nitroarenes (21 examples) under relatively mild conditions. The high catalytic performance and durability is attributed to the synergistic effects between each component, the unique structure of graphene layers-coated Co^0, and the electronic activation of doped nitrogen. Density functional calculations indicate that the inner Co^0 core and N species on the carbon shell can significantly decrease the dissociation energies of H_2, giving evidence of the ability of carbon shell in the hybrids to enable H_2 activation. These results open up an avenue to design more powerful low-cost catalysts for industrial applications.

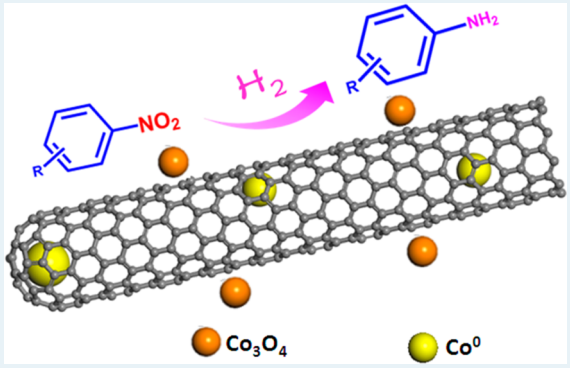

KEYWORDS: *chemoselective hydrogenation, heterogeneous catalyst, metallic cobalt, nitroarenes, nitrogen*

1. INTRODUCTION

Catalytic reduction reactions at nanoparticle surfaces constitute one of the most important operations for the conversion of chemical raw materials and in the production of highly valuable chemicals.[1,2] Development of new materials holds the key to fundamental advances in catalysis, both of which are vital in order to meet the challenge of environmental and energy crises.[3−5] Functionalized amines are industrially important intermediates for the manufacture of pharmaceuticals, agrochemicals, dyes, and fine chemicals.[6,7] The general method for the synthesis of anilines is the reduction of aromatic nitro compounds.[8−12] However, such processes cause environmental issues or selectivity problems. Undoubtedly, selective catalytic hydrogenations with hydrogen as the reductant represent one of the most critical technologies in chemical industry.

In terms of industrial applications, the careful design of heterogeneous catalysts instead of homogeneous ones is prevailing for the ease of their separation and recycling. However, the noble metals are often not chemoselective and they must be modified with suitable additives to improve selectivity, but mostly at the cost of activity.[13−16] Moreover, the additives also cause environmental issues. Breakthrough in supported Au nanoparticles (NPs) provided new opportunities for the selective hydrogenation of nitroarenes.[17−22] Even so, it remains a grand challenge to realize commercialization because of the risk in supply and volatile price. As a response, intensive research studies have been devoted to designing heterogeneous catalysts based on earth-abundant metals, such as Fe, Co, and Ni.[23−27] Although base metals are abundant and inexpensive, sintering or leaching of base metals (e.g., Co) cause irreversible deactivation of the catalysts under liquid-phase conditions.[28] Therefore, new strategies to develop stable, easy-to-handle, highly active, and selective base-metal catalysts without the use of any additives are highly necessary.

Nitrogen-containing nanostructured carbon materials, which possess enhanced chemical, electrical, and functional properties, are potentially of great technological interest for the development of a catalytic system.[11,29,30] Though nitrogen-doped graphene and carbon nanotubes (CNTs) can be applied into the reduction of 4-nitrophenol[31] and nitrobenzene,[32] strong reductants such as $NaBH_4$, hydrazine hydrate, among others, rather than H_2, were inevitably used, albeit still achieving inferior activity and limited reaction scope. The reason may be that carbon material with highly graphited sp^2 carbon is rather chemically inert to H_2.[33,34]

To overcome the limitations mentioned above, we speculate that the combination of N-doped carbon nanotubes (NCNTs) and first-row transition metals may lead to a successful

Received: April 8, 2015
Revised: July 2, 2015
Published: July 3, 2015

DOI: 10.1021/acscatal.5b00737
ACS Catal. 2015, 5, 4783−4789

integration of the properties of the two components in the new hybrid materials, which may present important features in catalysis.[35,36] Herein, we report a novel and straightforward method to prepare cobalt and NCNTs hybrids through self-assembly of inexpensive starting materials, that is, D-glucosamine hydrochloride (GAH), melamine, and $Co(NO_3)_2{\cdot}6H_2O$. The nanohybrids serve as highly active, selective, and stable catalysts for the hydrogenation of nitro compounds. Full conversion of various nitro substrates with excellent selectivity (>99% for most of the cases) toward the respective amines were achieved. Density functional theory (DFT) calculations indicated that the introduction of Co^0 and N dopants can simultaneously tune the inert graphene layer to be active in H_2 activation by lowering its dissociation energy, thus promoting the selective hydrogenation. The result challenges the traditional assumption that carbon usually is considered to be inert in H_2 activation.

2. RESULTS AND DISCUSSION

2.1. Fabrication and Characterization of Catalysts. The overall synthetic strategy was illustrated in Figure 1. Briefly, the

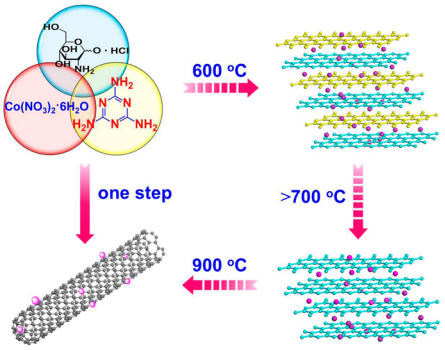

Figure 1. Overall synthetic procedure of CoO_x@NCNTs hybrids.

hybrids were achieved by simple thermal condensation of GAH, melamine, and $Co(NO_3)_2{\cdot}6H_2O$ at 900 °C. A holding sequence at 600 °C resulted in a sandwich-like structure, during which melamine thoroughly polymerized to form graphitic carbon nitride and GAH was condensed to form carbon skeleton in the interlayer of the carbon nitride.[37,38] The generated metal NPs were confined within the sandwich layers. High-temperature (>700 °C) annealing led to the thermal decomposition of carbon nitride, and cobalt-based NPs catalyzed the growth of NCNTs,[39] thus producing the hybrids (denoted as CoO_x@NCNTs). For comparisons, $Co(NO_3)_2$/GAH, $Co(NO_3)_2$/melamine, $Co(NO_3)_2$/glucose, and $Co(NO_3)_2$/commercial-CNTs were treated under identical conditions, and the composites obtained were named CoO_x@GAH, CoO_x@M, CoO_x@G, and CoO_x@CNTs, respectively.

The morphology and microstructures of CoOx@NCNTs were unambiguously characterized by scanning electron microscopy (SEM) and high-resolution transmission electron microscopy (HRTEM). The hybrids are made of several μm long and 50−100 nm thick multiwalled carbon nanotubes (Figure 2a,b). Most NPs dispersed effectively with a mean size of 12.9 nm by counting >300 NPs. In addition, a few particles are aggregated in the end point of the NCNTs. A preliminary analysis of the phenomenon is that the nanocrystals may be dispersed effectively in the polymerization process of melamine and GAH. The doped nitrogen atoms will anchor the NPs and protect them from agglomeration. The lattice spacing outside of NCNTs were measured to be 0.242 and 0.283 nm, which are in good agreement with that of crystalline Co_3O_4 (Figure 2c). Interestingly, the structure of nitrogen-doped carbon-coated NPs can be observed in Figure 2d, and the lattice fringes of NPs were assigned to the (111) facet of the Co^0 crystal. Although Co^0 is easily oxidized in air, it is exceptionally stable in CoO_x@NCNTs, suggesting the protective effect of the nitrogen-doped graphene layers.

The presence of Co_3O_4, Co^0, and crystalline carbon was further corroborated by powder X-ray diffraction (XRD). A pronounced diffraction peak at 26° and a weak reflection around 43° appeared in Figure 3b, which were ascribed to the (002) and (100) reflection of the graphitic-type lattice. The diffraction peaks at 31.3°, 36.9° could be assigned to the (220) and (311) planes of Co_3O_4 nanocrystal (PDF 42-1467). Besides, the diffraction peaks at 44.2° and 51.5° were recorded, which are the characteristic (111) and (220) reflections of cubic Co, respectively (PDF 15-0806). X-ray photoelectron spectroscopy (XPS) investigations confirmed that CoO_x@NCNTs contained C, N, Co, and O as the main elements (Figure S1 in the Supporting Information). As manifested in Figure 3c, two core-level signals located at ∼780 and 796 eV were attributed to Co $2p_{3/2}$ and Co $2p_{1/2}$, respectively. The peaks around 780 and 795.6 eV were assigned to Co_3O_4 phase, whereas those around 778.4 and 793.2 eV were in accordance with the formation of Co^0. Particularly worth mentioning was that a higher abundance of Co^{3+} species on the surface of CoO_x@NCNTs compared with CoO_x@G (Figure S2), implying that a strong interaction exists between Co_3O_4 and nitrogen-doped carbon skeleton through Co−O−C and Co−N−C bonds, which accordingly leads to a lower electron density at the Co site.[40] The textural properties of CoO_x@NCNTs were measured by N_2 adsorption−desorption analysis. The adsorption isotherm resembled type IV with a hysteresis loop, corresponding to the existence of mesopores (Figure 3a). The specific surface areas were calculated to be 254 $m^2\ g^{-1}$. Further insights into the structural and electronic properties of the nanohybrids were gained from Raman spectroscopy. Two well-defined peaks located at 1350 and 1580 cm^{-1} in Figure 3d could be assigned to typical D- and G-bands of carbon, respectively.[41] Other peaks were recorded and can be assigned to the Raman-active modes (A_{1g}, E_g, F_{2g}) of Co_3O_4.[42]

The obvious N 1s, C 1s spectra, and elemental analysis demonstrated that N has been incorporated into the system successfully (Table S1, Figure S3). Scanning TEM (STEM) and elemental mapping analyses of CoO_x@NCNTs disclosed that C, N, Co, and O species were uniformly distributed in the entire skeletal framework (Figure S4). All the investigations show that in situ-generated Co^0, Co_3O_4, and NCNTs together constitute CoO_x@NCNTs through one-pot synthesis.

2.2. Screening of Catalysts. To gain insight into the synergistic effect of each component, a series of control experiments based on the hydrogenation of the benchmark substrate nitrobenzene were performed. Commercial Co^0 worked in the hydrogenation of nitrobenzene but showed poor selectivity, and the bulk Co_3O_4 was completely inactive for the reaction (Table 1, entries 1 and 2). Commercially available CoO_x@CNTs acquired negligible yield, implying the existence of notable cooperative effect of the components in CoO_x@NCNTs (Table 1, entry 3). What is more, the catalysts, CoO_x@M, CoO_x@GAH, and carbon all gave indeed low yield or even no activity (Table 1, entries 4−6). We speculated that melamine, GAH, and $Co(NO_3)_2{\cdot}6H_2O$ are all indispensible in the

DOI: 10.1021/acscatal.5b00737
ACS Catal. 2015, 5, 4783−4789

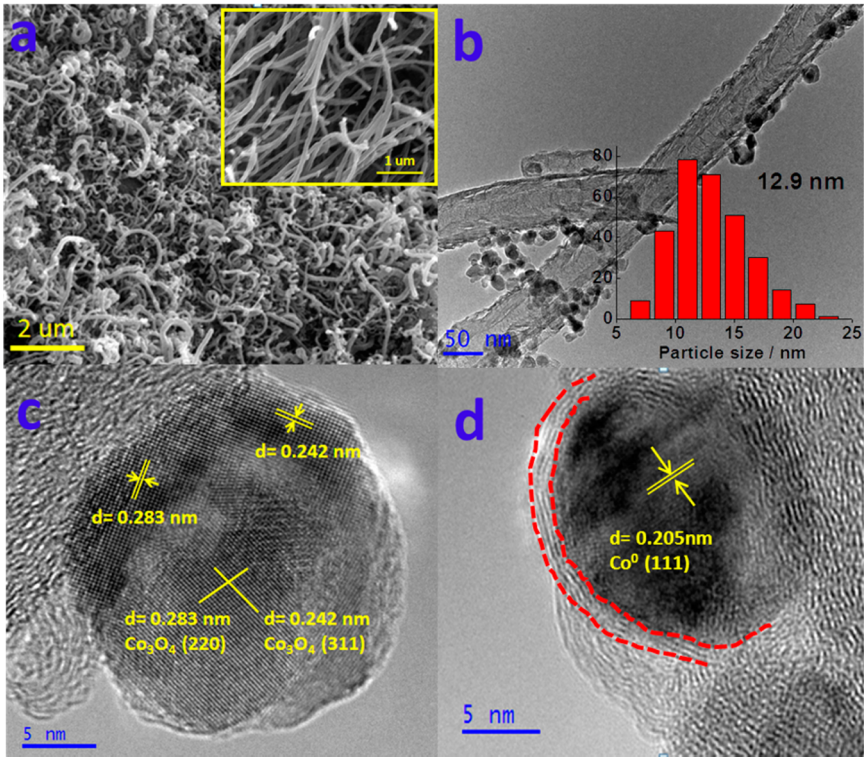

Figure 2. Representative SEM image (a), TEM image (b), and HRTEM images (c, d) of CoO_x@NCNTs. Inset (a) is magnification of the SEM image, and inset (b) is metal particle size distribution histogram.

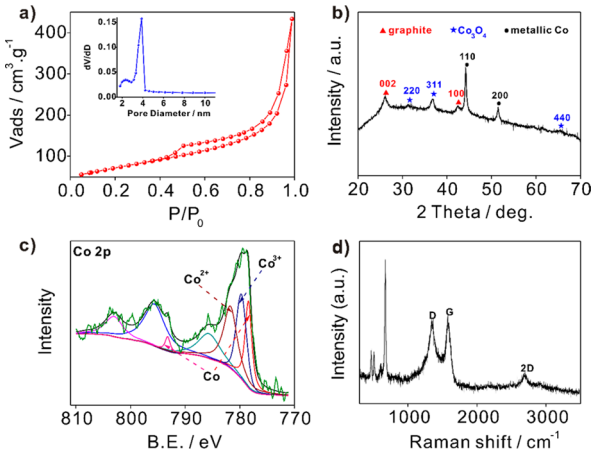

Figure 3. (a) Adsorption/desorption isotherms, (b) XRD patterns, (c) XPS spectrum, (d) Raman spectrum of the parent CoO_x@NCNTs. The inset in (a) is the pore size distribution.

Table 1. Catalytic Hydrogenation of Nitrobenzene[a]

entry	catalyst	time (h)	conv. (%)[b]	yield (%)[b]
1	Co^0	2.5	8	4
2	Co_3O_4	2.5	<1	0
3	CoO_x@CNTs	2.5	2	2
4	carbon[c]	2.5	<1	0
5	CoO_x@M	2.5	15	9
6	CoO_x@GAH	2.5	17	12
7	CoO_x@G	2.5	9	6
8	CoO_x@NCNTs	2.5	96	96
9	CoO_x@NCNTs	3	>99	98
10	CoO_x@NCNTs[d]	2.5	48	48

[a]Reaction conditions: 1 mmol nitrobenzene, 4.0 mol % Co, 5 mL of CH_3CH_2OH, 110 °C, 3 MPa H_2, 2.5 h. [b]Determined by GC (internal standard: n-dodecane). [c]Carbon is obtained from the calcination of GAH and melamine at 900 °C. [d]The catalyst was pyrolyzed at 1000 °C for 1 h.

fabrication of active catalysts and directly related to the catalytic performance. The surface area and total pore volume of CoO_x@M, CoOx@GAH, and CoO_x@G decreased dramatically compared with CoO_x@NCNTs, which may be a reason for the conspicuous loss in activity (Table S2, Figure S6). Moreover, it is generally accepted that the dispersion and the mean size of NPs may affect the catalytic activity greatly.[43] TEM images (Figure S7) validate that the supported NPs of above catalysts are larger than CoO_x@NCNTs, verifying the confinement effect of the sandwich-like structure derived from the polymerization of GAH and melamine. It must be noted that the nitrogen-free catalyst (CoO_x@G) exhibits the worst catalytic activity (Table 1, entry 7), which may be due to the much larger particle size (Table S2). These observations appear to manifest the doped nitrogen atoms play a crucial role in our system. The versatile nitrogen can provide more surface nucleation sites and promote the formation of some individual sections around the N-rich sites,[44] allowing efficient anchoring of metal NPs.[45]

Apart from the structural beneficial effects, the nitrogen functional groups also greatly affect the chemical state of the supported NPs. XRD results show that the diffraction peaks of Co^0 are evident in CoO_x@M and CoO_x@GAH but almost invisible for CoO_x@G (Figure S8). Instead, more characteristic peaks of Co_3O_4 occurred in the nitrogen-free catalyst, suggesting that the nitrogen species can promote the formation of Co^0. Briefly, the promoting effect of the nitrogen atoms leading to smaller particle size and more Co^0 may be responsible for the higher catalytic activity.

DOI: 10.1021/acscatal.5b00737
ACS Catal. 2015, 5, 4783−4789

Gratifyingly, the kinetic curves of the reaction (Figure S9) reveal that there is no significant formation of nitroso or polymerized products in our system, which suggests that the reaction may involve the direct hydrogenation of nitrobenzene to aniline.[46] The outstanding performance points to the high potential of the catalyst in industrial applications. Additionally, the reaction conditions were systematically optimized through variation of the pressure, temperature, and solvent with the results listed in Table S3.

2.3. Reusability of the Catalyst and Catalytic Active Sites Analysis. Catalyst stability and the feasibility of reuse is a key attraction to robust heterogeneous catalysts. To that end, we tested the catalytic activity of CoO_x@NCNTs in successive runs and compiled the results in Figure 4a. Unfortunately, the yield of

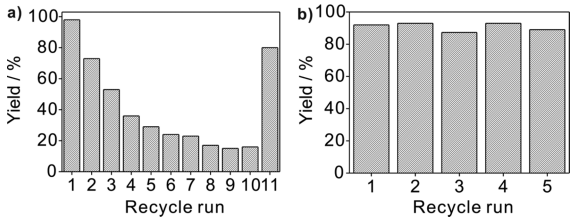

Figure 4. (a) Reuse of CoO_x@NCNTs (4 mol % Co), 3 h up to 10th recycle and 12 h for 11th cycle, and (b) reuse of Co^0@NCNTs (2.4 mol % Co), 3 h for each recycle. Reaction conditions: 110 °C, 3 MPa H_2.

aniline decreased gradually then leveled off despite maintenance of perfect chemoselectivity throughout. Nevertheless, the activity can recover through extending the reaction time (for the 11th cycle). TEM studies of the catalyst after 11 time recycles revealed the particle size of ~13.6 nm (Figure S10), almost the same as the fresh one, which indicated that the catalyst is aggregation-free after reuse. The decreased activity of CoO_x@NCNTs was primarily due to metal leaching as manifested in Table S4 during the recycle reactions. In a separate test, 51% conversion of nitrobenzene was achieved within 1.5 h at 110 °C. Then we collected the liquid phase by centrifugation. The amount of nitrobenzene remained almost unchanged after a further 1.5 h reaction, hinting that the leached species in the filtrate made no contribution to the conversion of nitrobenzene. More importantly, the variation of the metal state in our system also had a significant effect on the catalytic activity. XRD results of the catalyst after the first use showed that only CoO and Co^0 reflections were recorded (Figure S11). The results suggested that Co_3O_4 in the fresh catalyst was totally converted to CoO in the first use. Besides, the Co^0 content in the fresh and recycled catalyst was determined by semiquantitative analysis of XPS. The Co^0 content increased slightly to 22.5% from 16.3% after 11 recycles (Table S2, S5). This suggests that CoO may be partly converted to Co^0, which makes the catalytic activity level off despite existence of leaching. To explain it clearly, hydrogen temperature-programmed reduction (H_2-TPR) was conducted. Two representative reduction peaks of Co_3O_4 were detected in CoO_x@NCNTs catalyst, which was extraordinarily lower than that of commercial Co_3O_4 (Figure S13), indicating the phase of Co_3O_4 in our system was very likely to be reduced by hydrogen under the reaction conditions. The results match well with the conclusion that Co_3O_4 can be readily converted to CoO. Meanwhile, the transformation from CoO to Co^0 is also possible.

The unexpected stability of Co^0 inspired us to investigate the catalyst in detail. Co^0 covered with nitrogen-doped graphene layers (denoted as Co^0@NCNTs) can be easily obtained by acid treatment of CoO_x@NCNTs. The HRTEM images (Figure S14) showed the complete coverage of Co^0 with graphene layers. Full yield of aniline was also achieved with Co^0@NCNTs (3 mol % Co) in 3 h (110 °C, 3 MPa H_2). It shows that Co^0@NCNTs perform better than CoO_x@NCNTs (Table 1, entry 9), indicating that Co^0 is even more effective than CoO_x for the hydrogenation of nitrobenzene. Upon raising the pyrolysis temperature to 1000 °C, there is an apparent decline in Co^0 content (determined from XPS analysis) (Table S2). SEM images showed that part of NCNTs decomposed and carbon spheres appeared (Figure S15). Meanwhile, the mean size of the cobalt-based NPs increased (Table S2). Correspondingly, the activity dropped dramatically, only furnishing 48% yield (Table 1, entry 10), reconfirming that Co^0 NPs and their uniform morphology gave a big boost to the performance of catalysts. What is more, Co^0@NCNTs can be recycled up to five times with unconspicuous loss of activity (Figure 4b), overcoming the poor durability of cobalt-based catalyst for the hydrogenation of nitrobenzene in liquid phase. Very clear cubic Co reflections were recorded for Co^0@NCNTs after five times use (Figure 5b),

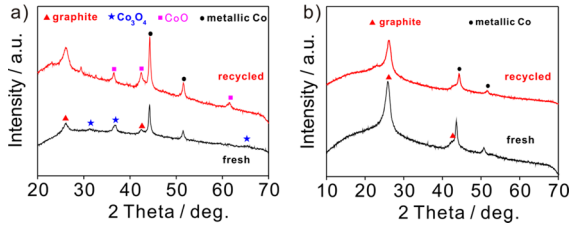

Figure 5. XRD patterns of the fresh and recycled catalysts, (a) CoO_x@NCNTs and (b) Co^0@NCNTs.

verifying the improved resistance of Co^0 against oxidation with the aid of nitrogen-doped graphene layers. Co^0@NCNTs exhibits superior heterogeneous catalytic performance in terms of selectivity, stability, and recyclability.

2.4. DFT Calculations of H_2 Activation. Generally, graphitic carbon deposited on transition metal is considered as catalyst poison due to the chemical inertness and physical blockage of surface active sites.[47] In contrast, the excellent activity of Co^0@NCNTs in this work shows a unique phenomenon to the activation of H_2 on the carbon shell outside, which is possibly attributed to the modification of the inner Co^0 core and N species on the carbon shell. To confirm the deduction, a first-principle calculation was performed. We studied the dissociation of H_2 on perfect graphene (GP), Co^0 with covered graphene (Co^0@GP), and Co^0 with covered graphitic N-doped graphene (Co^0@NGP), respectively. As is illustrated in Figure 6, graphene, i.e. the carbon basal surface alone is rather inert to H_2, giving a dissociation energy of 1.85 eV. Once the graphene is deposited on Co^0, the dissociation energy is

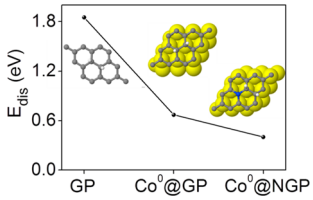

Figure 6. Dissociation energies of H_2 on different catalysts. Insets are the optimized dissociative structures. Color code: cobalt is yellow, carbon is gray, nitrogen is blue, and hydrogen is white.

DOI: 10.1021/acscatal.5b00737
ACS Catal. 2015, 5, 4783−4789

significantly reduced, which implies that Co^0 can improve the activity of the graphene layer in H_2 activation. What is more, the activity of Co^0@GP is further improved by N doping with a dissociation energy of 0.40 eV. The optimized dissociative structures of the three catalysts are shown in Figure 6. The calculated results match well with the experimental phenomenon. To illustrate the origin of the improved catalytic activity, the electronic structures of the catalysts were investigated. There is an electron transfer of net 0.05 e from the coated Co^0 to each carbon atom of the carbon shell in average, making the carbon shell more electron-rich, which would be beneficial to dissociate H_2 because the activation process involves the electron injection to the H 1s antibonding state. For Co^0@NGP, though the carbon atom gets no net electron transfer in average due to the bigger electronegativity of N, the electron distribution of the carbon shell changes obviously. As shown in Figure S16, some of the carbon atoms in N-doped carbon shell get more electrons than the undoped one. This may explain the reason why N doping further enhances the catalytic activity. Note that only the influence of Co^0 and N to the activation of H_2 on the graphene is considered because the real active sites on the catalyst are still debated.[48,49] A more in-depth work on the reaction mechanism is to be further investigated.

2.5. Hydrogenation of Substituted Nitroarenes. With the optimized reaction conditions in hand, we were keen to test the general scope of CoO_x@NCNTs in the hydrogenation of nitroarenes with diverse substituent groups. Pleasingly, the catalyst was found to be a highly active and almost exclusively selective catalyst for the hydrogenation of substituted nitroarenes. Apart from nitrobenzene (Table 2, entry 1), the substituted nitrobenzene having electron-donor or electron-acceptor groups were also furnished with excellent yields (Table 2, entries 2−8). Notably, halogen-substituted nitroarenes proceeded smoothly to the respective haloaromatic amines without any dehelogenation (Table 2, entries 9−14).

Moreover, CoO_x@NCNTs also showed impressive chemoselectivity in the hydrogenation of the most-challenging substrates bearing other easily reducible groups. The reducible functional groups in aromatic nitro substrates such as nitrile, aldehyde, keto, amide and alkene (Table 2, entries 15−21) remained totally unaffected, thus giving the corresponding amines selectively. These results highlight again the distinctive difference between CoO_x@NCNTs and the noble metal catalysts in the selective hydrogenation of substituted aromatic compounds, with the cobalt catalyst displaying superior selectivity in general.

3. CONCLUSIONS

In summary, we developed a scalable, environmentally benign, and straightforward strategy for the synthesis of Co^0/Co_3O_4@NCNTs. The hybrids display excellent catalytic performance for the hydrogenation of nitroarenes into the corresponding anlines. This work represents a clear demonstration of the cooperative effect of each component in the ternary catalyst, where the sandwich-like structure derived from the polymerization of melamine and GAH plays a crucial role in the uniform dispersion of NPs and the doped nitrogen atoms can promote the formation of Co^0. DFT calculations indicate that the Co^0 and N atoms in the hybrids can simultaneously tune the inert graphene layer to be active in H_2 activation by lowering its dissociation energy. The finding opens up an avenue to design more powerful catalysts through coating of metal NPs with graphene layers. Moreover, the synthesis strategy provides a versatile platform to introduce various metal species on nitrogen-doped carbon with targeted and improved properties for diverse catalytic reactions. Work along this line is currently underway.

Table 2. Chemoselective Hydrogenation of Various Substituted Nitroarenes[a]

entry	substrate	product	time (h)	selectivity (%)[b]	yield (%)[b]
1			3	>99	>99
2			3	>99	>99
3[c]			6	>99	>99
4			8	99	99
5[c]			8	>99	>99
6			6	>99	>99
7			10	>99	>99
8[c]			15	>99	>99
9			4	>99	>99
10			4	>99	>99
11			4	>99	>99
12			4	>99	>99
13			10	>99	>99
14			12	96	96
15			6	95	95
16			5	>99	>99
17			4	>99	>99
18			6.5	>99	>99
19			5	98	98
20			10	>99	>99
21[c]			12	98	98

[a]Reaction conditions: 1 mmol nitroarene, 4.0 mol % Co, 5 mL of CH_3CH_2OH, 110 °C, 3 MPa H_2, >99% conversion observed in all cases. [b]Determined by GC (internal standard: n-dodecane). [c]0.5 mmol substrate.

4. EXPERIMENTAL SECTION

4.1. Materials and Catalysts Preparation. D-Glucosamine hydrochloride, melamine, glucose, $Co(NO_3)_2{\cdot}6H_2O$, cobalt powder, and Co_3O_4 were purchased from Aladdin. Commercial

DOI: 10.1021/acscatal.5b00737
ACS Catal. 2015, 5, 4783−4789

CNTs were used as received from Shenzhen Nanotech Port Co., Ltd. Unless otherwise stated, all solvents and chemicals used were of commercially available analytical grade and used without further treatment. All gases (H_2, N_2) used for catalyst preparation and reaction process were ultrahigh purity.

The synthesis of CoO_x@NCNTs involves self-assembly of GAH, melamine, and $Co(NO_3)_2{\cdot}6H_2O$. In a typical synthesis, a solid mixture of 1 g of GAH, 40 g of melamine, and 0.95 g of $Co(NO_3)_2{\cdot}6H_2O$ was grinded into powder. Then the homogeneous mixture was transferred into a crucible, directly heated to 600 °C at a rate of 2.5 °C min^{-1}, and kept at 600 °C for 1 h by flowing N_2 of 400 mL min^{-1}. The temperature of the material was further increased to 900 °C (2.5 °C min^{-1}) for 1 h. After that, the samples were cooled to room temperature under N_2 ambient. Finally, the products were collected from the crucible. For comparison, CoO_x@GAH, CoO_x@M, CoO_x@G, and CoO_x@CNTs were obtained through the same protocol. Co^0@NCNTs was acquired by acid treatment of CoO_x@NCNTs (1 M HNO_3 for 48 h at room temperature). The sample pyrolyzed at 1000 °C was first heated at 600 °C at a rate of 2.5 °C min^{-1} and kept at 600 °C for 1 h. Then the material was further raised to 1000 °C (2.5 °C min^{-1}) for 1 h by flowing N_2 of 400 mL min^{-1}.

4.2. Characterization Analyses. SEM (LEO 1550) was applied to visualize the morphology of the catalysts. TEM images were obtained from a Hitachi H7700 transmission electron microscope with CCD imaging system on an acceleration voltage of 100 kV. HRTEM, STEM-HAADF, and STEM-EDX were performed on Tecnai G2 F30 S-Twin at an acceleration voltage of 300 kV. Nitrogen adsorption analysis was performed at 77 K using a Micromeritics ASAP 2020 to access the surface areas and pore distributions. The Brunauer−Emmett−Teller (BET) method was used to calculate the specific surface area (S_{BET}). Total pore volumes (V_{total}) were calculated from the amount of nitrogen adsorbed at a relative pressure, P/P_0 of 0.97. The pore size distribution (PSD) plot was recorded from the desorption branch of the isotherm based on the Barrett−Joyner−Halenda (BJH) model. XRD patterns were collected at room temperature with 2 θ scan range between 5° and 90° using a wide-angle X-ray diffraction (Model D/tex-Ultima TV, Rig-aku, Japan) equipped with Cu Kα radiation (40 kV, 30 mA, 1.54 Å). The Co_3O_4 sizes were calculated from the Scherrer formula according to the 311 ($2\theta = 36.9$) diffraction lines in wide-angle XRD. XPS information was obtained with an ESCALAB MARK II spherical analyzer using an aluminum anode (Al 1486.6 eV) X-ray source. The Raman spectra were collected on a Raman spectrometer (JY, HR 800) using a 514 nm laser. The element analysis was measured on a Vario El elemental analyzer. The Co content was determined by ICP-AES (PerkinElmer Optima OES 8000), and aqua regia was used to dissolve the sample. H_2-TPR was conducted with a FINESORB-3010 apparatus equipped with a thermal conductivity detector (TCD). Before a TPR run, catalysts were pretreated in Ar at 423 K for 1 h. TPR was performed under a flow of 10% H_2/Ar gas mixture at a flow rate of 10 sccm with a temperature ramp of 10 °C/min.

4.3. Catalytic Procedure and Recycling. The high-pressure hydrogenation reactions were carried out in a 50 mL stainless-steel autoclave with an external temperature and stirring controller. In a typical experiment, the autoclave was charged with nitrobenzene (123 mg, 1 mmol), the internal standard (dodecane, 110 mg), the cobalt catalyst (CoO_x@NCNTs, 8.7 mg, 4 mmol %), and the green solvent ethanol (5 mL). The reactor was purged with H_2 to remove the air for three times and then sealed tight and pressurized to 3 MPa H_2. The autoclave was placed into an oil-bath (placed 15 min before counting the reaction time in order to obtain reaction temperature) preheated at 120 °C, and the reactions were stirred at 1000 rpm at 110 °C. After the reaction, the reactor was placed into a water bath and cooled to room temperature. The remaining H_2 was carefully vented, and the reaction mixture was removed for further analysis. The mixture was diluted with 25 mL of ethanol followed by centrifugation. The contents of the mixture were analyzed on GC (Shimadzu, GC-2014) equipped with a Rtx-1071 column and the products were identified by GC-MS (Agilent Technologies, GC 6890N, MS 5970).

For recycling study, the hydrogenation reaction was performed with 2.3 mmol scale (282 mg of nitrobenzene, 230 mg of dodecane, 20 mg of CoO_x@NCNTs, and 10 mL of ethanol), maintaining the same reaction conditions as mentioned above except using the recovered catalyst. The catalyst was recovered by centrifugation, washed three times with ethanol, and dried at 70 °C overnight and then used for the next run without any reactivation or purification.

4.4. DFT Calculations. The calculations are performed by using periodic, spin-polarized DFT as implemented in Vienna ab initio program package (VASP)[50,51] with an electron−ion interaction described by the projector augmented wave (PAW) method, which was proposed by Blöchl[52] and implemented by Kresse.[53] RPBE functional[54] is used as exchange−correlation functional approximation with an energy cutoff of 400 eV for a plane wave basis. A 3 × 3 × 1 k-points is used for the Brillouin zone sampling for structure optimizing, and a 5 × 5 × 1 k-points for the electronic structure calculation. The graphene sheet (GP) was modeled by a 3 × 3 unit cell with 9 carbon atoms and a vacuum space of 13 Å between adjacent slabs was set. Co^0@GP was modeled from GP with 3 (111) Co layers under covered. Co^0@NGP was modeled from Co^0@GP with a graphitic-doped nitrogen on the graphene layer (Figure S17). For GP catalyst, all the atoms in the cell were allowed to relax during the structure optimization. For Co^0@GP and Co^0@NGP catalysts, the outer two layers were allowed to relax and the two bottom layers were fixed. The optimization is stopped when the force residue on the atom is smaller than 0.02 eV/Å. The dissociation energy is defined as

$$E_{dis} = E_{tot} - E_{slab} - E_{H_2} \quad (1)$$

where E_{tot} is the total energy after the dissociation of H_2 on the catalyst; E_{slab} is the energy of the clean slab alone; and E_{H_2} is the energy of H_2 in the gas phase.

■ ASSOCIATED CONTENT

Supporting Information

The Supporting Information is available free of charge on the ACS Publications website at DOI: 10.1021/acscatal.5b00737.

Detailed analysis of the fresh catalysts and recycled catalysts, optimization parameters for the hydrogenation of nitrobenzene, kinetic curves for nitrobenzene hydrogenation, and supplementary figures (PDF)

■ AUTHOR INFORMATION

Corresponding Author

*E-mail: chemwy@zju.edu.cn. Tel.: 86-571-88273551. Fax: +86-571-87951895.

Author Contributions

‡These authors contributed equally (Z.W. and J.W.).

DOI: 10.1021/acscatal.5b00737
ACS Catal. 2015, 5, 4783−4789

Notes

The authors declare no competing financial interest.

■ ACKNOWLEDGMENTS

Financial support from the National Natural Science Foundation of China (21376208), the Zhejiang Provincial Natural Science Foundation for Distinguished Young Scholars of China (LR13B030001), the Specialized Research Fund for the Doctoral Program of Higher Education (J20130060), the Fundamental Research Funds for the Central Universities, the Program for Zhejiang Leading Team of S&T Innovation, and the Partner Group Program of the Zhejiang University and the Max-Planck Society are greatly appreciated.

■ REFERENCES

(1) Su, Y.; Lang, J.; Li, L.; Guan, K.; Du, C.; Peng, L.; Han, D.; Wang, X. *J. Am. Chem. Soc.* **2013**, *135*, 11433−11436.
(2) Gärtner, D.; Welther, A.; Rad, B. R.; Wolf, R.; Jacobi von Wangelin, A. *Angew. Chem., Int. Ed.* **2014**, *53*, 3722−3726.
(3) Arico, A. S.; Bruce, P.; Scrosati, B.; Tarascon, J. M.; Van Schalkwijk, W. *Nat. Mater.* **2005**, *4*, 366−377.
(4) Jin, H.; Wang, J.; Su, D.; Wei, Z.; Pang, Z.; Wang, Y. *J. Am. Chem. Soc.* **2015**, *137*, 2688−2694.
(5) Su, D.; wang, J.; Jin, H.; Gong, Y.; Li, M.; Pang, Z.; Wang, Y. *J. Mater. Chem. A* **2015**, *3*, 11756−11761.
(6) Downing, R. S.; Kunkeler, P. J.; van Bekkum, H. *Catal. Today* **1997**, *37*, 121−136.
(7) Blaser, H. U.; Steiner, H.; Studer, M. *ChemCatChem* **2009**, *1*, 210−221.
(8) Wienhöfer, G.; Sorribes, I.; Boddien, A.; Westerhaus, F.; Junge, K.; Junge, H.; Llusar, R.; Beller, M. *J. Am. Chem. Soc.* **2011**, *133*, 12875−12879.
(9) Shalom, M.; Molinari, V.; Esposito, D.; Clavel, G.; Ressnig, D.; Giordano, C.; Antonietti, M. *Adv. Mater.* **2014**, *26*, 1272−1276.
(10) Bae, J. W.; Cho, Y. J.; Lee, S. H.; Yoon, C.-O. M.; Yoon, C. M. *Chem. Commun.* **2000**, 1857−1858.
(11) Liu, R.; Mahurin, S. M.; Li, C.; Unocic, R. R.; Idrobo, J. C.; Gao, H. J.; Pennycook, S. J.; Dai, S. *Angew. Chem., Int. Ed.* **2011**, *50*, 6799−6802.
(12) Jagadeesh, R. V.; Wienhofer, G.; Westerhaus, F. A.; Surkus, A. E.; Pohl, M. M.; Junge, H.; Junge, K.; Beller, M. *Chem. Commun.* **2011**, *47*, 10972−10974.
(13) Corma, A.; Serna, P.; Concepcion, P.; Calvino, J. J. *J. Am. Chem. Soc.* **2008**, *130*, 8748−8753.
(14) Tafesh, A. M.; Weiguny, J. *Chem. Rev.* **1996**, *96*, 2035−2052.
(15) Blaser, H.-U.; Siegrist, U.; Steiner, H.; Studer, M. In *Aromatic Nitro Compounds: Fine Chemicals through Heterogeneous Catalysis*; Sheldon, R. A.; van Bekkum, H., Eds.; Wiley-VCH: Weinheim, 2001; pp 389−406.
(16) Siegrist, U.; Baumeister, P.; Blaser, H.-U. In *Catalysis of Organic Reactions*; Herkes, F. E., Ed.; Marcel Dekker: New York, 1998, Vol. *75*, pp 207−219.
(17) Corma, A.; Serna, P. *Science* **2006**, *313*, 332−334.
(18) Boronat, M.; Concepcion, P.; Corma, A.; Gonzalez, S.; Illas, F.; Serna, P. *J. Am. Chem. Soc.* **2007**, *129*, 16230−16237.
(19) Grirrane, A.; Corma, A.; Garcia, H. *Science* **2008**, *322*, 1661−1664.
(20) He, L.; Wang, L.-C.; Sun, H.; Ni, J.; Cao, Y.; He, H.-Y.; Fan, K.-N. *Angew. Chem., Int. Ed.* **2009**, *48*, 9538−9541.
(21) Li, S.-C.; Diebold, U. *J. Am. Chem. Soc.* **2009**, *132*, 64−66.
(22) Liu, X.; Li, H.-Q.; Ye, S.; Liu, Y.-M.; He, H.-Y.; Cao, Y. *Angew. Chem., Int. Ed.* **2014**, *53*, 7624−7628.
(23) Bullock, R. M. *Science* **2013**, *342*, 1054−1055.
(24) Westerhaus, F. A.; Jagadeesh, R. V.; Wienhofer, G.; Pohl, M. M.; Radnik, J.; Surkus, A. E.; Rabeah, J.; Junge, K.; Junge, H.; Nielsen, M.; Bruckner, A.; Beller, M. *Nat. Chem.* **2013**, *5*, 537−543.
(25) Wu, Y. G.; Wen, M.; Wu, Q. S.; Fang, H. *J. Phys. Chem. C* **2014**, *118*, 6307−6313.
(26) Jagadeesh, R. V.; Surkus, A. E.; Junge, H.; Pohl, M. M.; Radnik, J.; Rabeah, J.; Huan, H. M.; Schunemann, V.; Bruckner, A.; Beller, M. *Science* **2013**, *342*, 1073−1076.
(27) Cantillo, D.; Baghbanzadeh, M.; Kappe, C. O. *Angew. Chem., Int. Ed.* **2012**, *51*, 10190−10193.
(28) Lee, J.; Jackson, D. H. K.; Li, T.; Winans, R. E.; Dumesic, J. A.; Kuech, T. F.; Huber, G. W. *Energy Environ. Sci.* **2014**, *7*, 1657−1660.
(29) Lee, J. S.; Wang, X.; Luo, H.; Baker, G. A.; Dai, S. *J. Am. Chem. Soc.* **2009**, *131*, 4596−4597.
(30) Wei, Z.; Gong, Y.; Xiong, T.; Zhang, P.; Li, H.; Wang, Y. *Catal. Sci. Technol.* **2015**, *5*, 397−404.
(31) Kong, X.-k.; Sun, Z.-y.; Chen, M.; Chen, C.-l.; Chen, Q.-w. *Energy Environ. Sci.* **2013**, *6*, 3260−3266.
(32) Gao, Y. J.; Ma, D.; Wang, C. L.; Guan, J.; Bao, X. H. *Chem. Commun.* **2011**, *47*, 2432−2434.
(33) Lee, E.-C.; Kim, Y. S.; Jin, Y. G.; Chang, K. *Phys. Rev. B: Condens. Matter Mater. Phys.* **2002**, *66*, 073415.
(34) Kong, L.; Enders, A.; Rahman, T. S.; Dowben, P. A. *J. Phys.: Condens. Matter* **2014**, *26*, 443001.
(35) Georgakilas, V.; Gournis, D.; Tzitzios, V.; Pasquato, L.; Guldi, D. M.; Prato, M. *J. Mater. Chem.* **2007**, *17*, 2679−2694.
(36) Li, X.-H.; Antonietti, M. *Chem. Soc. Rev.* **2013**, *42*, 6593−6604.
(37) Li, X.-H.; Kurasch, S.; Kaiser, U.; Antonietti, M. *Angew. Chem., Int. Ed.* **2012**, *51*, 9689−9692.
(38) Wang, J.; Xu, Z.; Gong, Y.; Han, C.; Li, H.; Wang, Y. *ChemCatChem* **2014**, *6*, 1204−1209.
(39) Wang, J.; Wei, Z.; Gong, Y.; Wang, S.; Su, D.; Han, C.; Li, H.; Wang, Y. *Chem. Commun.* **2015**, DOI: 10.1039/C5CC02593A.
(40) Liang, Y. Y.; Li, Y. G.; Wang, H. L.; Zhou, J. G.; Wang, J.; Regier, T.; Dai, H. J. *Nat. Mater.* **2011**, *10*, 780−786.
(41) Zou, X. C.; Huang, X. C.; Goswami, A.; Silva, R.; Sathe, B. R.; Mikmekova, E.; Asefa, T. *Angew. Chem., Int. Ed.* **2014**, *53*, 4372−4376.
(42) Nie, R. F.; Shi, J. J.; Du, W. C.; Ning, W. S.; Hou, Z. Y.; Xiao, F. S. *J. Mater. Chem. A* **2013**, *1*, 9037−9045.
(43) Coq, B.; Figueras, F. *Coord. Chem. Rev.* **1998**, *178-180*, 1753−1783.
(44) Lepró, X.; Terrés, E.; Vega-Cantú, Y.; Rodríguez-Macías, F. J.; Muramatsu, H.; Kim, Y. A.; Hayahsi, T.; Endo, M.; Torres, R. M.; Terrones, M. *Chem. Phys. Lett.* **2008**, *463*, 124−129.
(45) Chen, P. R.; Yang, F. K.; Kostka, A.; Xia, W. *ACS Catal.* **2014**, *4*, 1478−1486.
(46) Corma, A.; Concepción, P.; Serna, P. *Angew. Chem., Int. Ed.* **2007**, *46*, 7266−7269.
(47) Yao, Y.; Fu, Q.; Zhang, Y. Y.; Weng, X.; Li, H.; Chen, M.; Jin, L.; Dong, A.; Mu, R.; Jiang, P.; Liu, L.; Bluhm, H.; Liu, Z.; Zhang, S. B.; Bao, X. *Proc. Natl. Acad. Sci. U. S. A.* **2014**, *111*, 17023−17028.
(48) Erokhin, A. V.; Lokteva, E. S.; Yermakov, A. Y.; Boukhvalov, D. W.; Maslakov, K. I.; Golubina, E. V.; Uimin, M. A. *Carbon* **2014**, *74*, 291−301.
(49) Yermakov, A. Y.; Boukhvalov, D. W.; Uimin, M. A.; Lokteva, E. S.; Erokhin, A. V.; Schegoleva, N. N. *ChemPhysChem* **2013**, *14*, 381−385.
(50) Kresse, G.; Furthmüller, J. *Comput. Mater. Sci.* **1996**, *6*, 15−50.
(51) Kresse, G.; Furthmüller, J. *Phys. Rev. B: Condens. Matter Mater. Phys.* **1996**, *54*, 11169−11186.
(52) Blöchl, P. E. *Phys. Rev. B: Condens. Matter Mater. Phys.* **1994**, *50*, 17953−17979.
(53) Kresse, G.; Joubert, D. *Phys. Rev. B: Condens. Matter Mater. Phys.* **1999**, *59*, 1758−1775.
(54) Hammer, B.; Hansen, L. B.; Nørskov, J. K. *Phys. Rev. B: Condens. Matter Mater. Phys.* **1999**, *59*, 7413−7421.

DOI: 10.1021/acscatal.5b00737
ACS Catal. 2015, 5, 4783−4789